Nanoscale

Accepted Manuscript

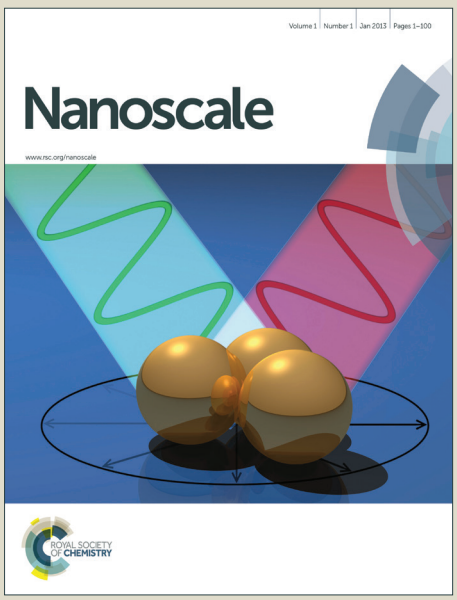

ROYAL SOCIETY OF CHEMISTRY

www.rsc.org/nanoscale

Nanoscale

RSCPublishing

COMMUNICATION

A facile route for growth of CNT on Si@hard carbon for conductive agent incorporating anodes for lithium-ion batteries

Cite this: DOI: 10.1039/x0xx00000x

Received 00th January 2012,
Accepted 00th January 2012

DOI: 10.1039/x0xx00000x

www.rsc.org/

Chanhoon Kim,[a] Sinho Choi,[a] Seungmin Yoo,[a] Dohyoung Kwon,[a] Seunghee Ko,[a] Ju-Myung Kim,[a] Sang-Young Lee,[a] Il-Doo Kim,[b] and Soojin Park[a]*

Conductive agent incorporating Si anodes consisting of directly grown carbon nanotubes on hard carbon encapsulating Si nanoparticles were prepared by one-pot chemical vapour deposition process. Owing to this fabulous structure, Si-based anodes exhibit excellent cycle retention and rate capability with a high-mass-loading of 3.5 mg cm^{-2}.

The ever-increasing concerns about global warming have stimulated intense interest in the development of both renewable energy sources and high efficiency energy storage devices.[1-5] Lithium-ion batteries (LIBs) have currently dominated the portable device market due to their advantages including: (i) high operating voltages, (ii) the lack of a memory effect, (iii) low self-discharge rates, (iv) relatively high energy and power densities compared to those of other conventional batteries such as lead-acid and nickel metal hydride.[6-9] However, rapidly growing electric vehicle market requires the development of LIBs possessing the high energy and power density which far surpass those of current LIBs. Commercialized graphite anodes deliver insufficient theoretical capacity of 372 mAh g^{-1} which is far below subminimum capacity for electric vehicles. In response to that trend, the conventional graphite anodes should be replaced with advanced anode materials.[4, 10-14]

In recent years, Si has received intensive attention as a next-generation anode material which is expected to facilitate drive the electric vehicles without sacrificing distance due to its incredibly high theoretical capacity (>3500 mAh/g at room temperature).[10, 15-18] However, its large volume expansion (>300 %) during lithiation process leads to a serious degradation of electric contact between active materials and conducting agents as well as current collector.[2, 19-22] Furthermore, the low electrical conductivity of Si requires the use of large amount of conductive agents which are not directly involved in faradaic reactions of LIBs. Therefore, the use of conductive agents should be minimized to incorporate more active materials into a fixed volume of electrode for high energy density.[23,24]

To alleviate the huge volume change of Si, a rich variety of attempts have been developed, such as nanostructuring of Si (e.g. nanoparticles, nanotubes, nanowires, hollow nanospheres etc.) and incorporating Si into the conductive buffer matrix (amorphous carbon, graphene, carbon nanotubes, etc.).[16, 25-35]

Among them, incorporating nanostructured Si into conductive buffer matrix can enhance both the electrical conductivity and alleviate a large volume change during cycling. Typically, the carbon has been widely used as buffer matrix for Si with several advantages like high electrical conductivity, long cycle life, and excellent rate performance.[36] However, most of Si/carbon (Si/C) composites have zero dimensional shapes which still require a large amount of conductive agents because they cannot develop sufficient electrical networks by themselves in electrodes.[37] Furthermore, nanopowder type conductive agents are inadequate to play a role of electrical networks between these zero dimensional shapes of Si/carbon composites. Therefore, introducing three-dimensional (3D) electrical networks directly on Si/C composites is advisable. As another approach, researchers tried to use commercially available carbon nanotubes (CNTs) as conductive supports for active materials, in which active materials were deposited or coated on the CNTs (active materials@CNTs).[38-40] In this case, however, only small amount of active materials can be loaded or coated on CNTs.

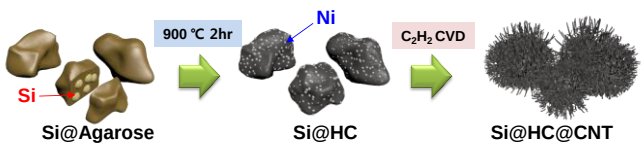

Fig. 1 Schematic illustration of a facile process of Si@HC@CNT synthesized via CVD method.

We herein report a new structure of Si anodes, consisting of directly grown carbon nanotubes (CNTs) on hard carbon (HC) encapsulating Si nanoparticles. The HC derived from natural polysaccharide provides effective conductive and buffer matrix for Si particles. Furthermore, directly grown CNTs on the surface of HC act as 3D electrical circuit between active materials without conductive agents. The electrodes are also composed of very high portion of active materials (90 wt%) and small portion of binder (10 wt%). This high energy density Si-based anode exhibits high initial coulombic efficiency (ICE) of 85.7% and excellent cycle retention after 500 cycles at a rate of 0.5C discharge/charge, which far surpasses the results of HC encapsulating Si anodes containing 10 wt% of conductive agents (Super P carbon black) (denoted as Si@HC/SP).

Schematic illustration of the facile process to produce Si@HC@CNT is shown in Fig. 1. Commercial Si nanoparticles (<150 nm) and nickel precursors ($Ni(NO_3)_2 \cdot 6H_2O$) were finely dispersed in the agarose hydrogel and subsequently, it was dried in a convection oven at 70 °C for 12 h. Agarose is one type of the natural polysaccharides which is extracted from seaweeds.[41] In our previous work, we demonstrated that the HC derived from agarose has microporous structure, which is favourable for rapid lithium diffusion, exhibits superior rate capability and very stable long-term cyclability.[36] Therefore, we chose agarose as HC source in order to encapsulate Si nanoparticles.

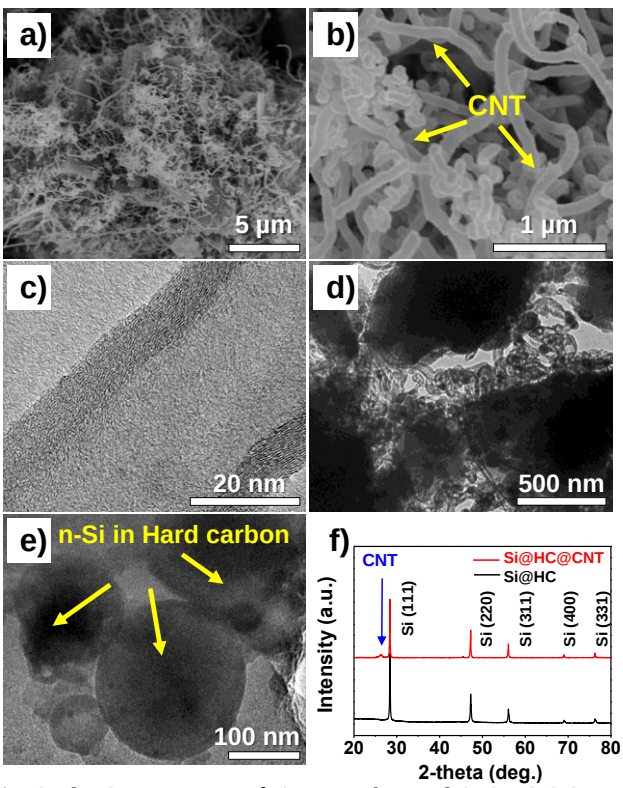

Fig. 2 The SEM images of a) as-synthesized Si@HC@CNT, b) the magnified Si@HC@CNT; TEM images of the c) CNT in Si@HC@CNT, d) as-synthesized Si@HC@CNT, and e) the magnified Si@HC@CNT. e) XRD patterns of Si@HC@CNT and Si@HC.

The Si@agaorse composites were simply carbonized at 900 °C for 2 h in a tube furnace with Ar flow. Meanwhile, Ni precursor in the Si@agarose composites were converted to nanosized Ni catalyst for CNTs growth during the carbonization process. Subsequently, the CNTs were grown using chemical vapour deposition via a tip-growth mechanism.[42-44] During the carbonization of Si@agarose composites, acetylene gas (C_2H_2: 10 % and Ar: 90 %) was flowed into the tube furnace at 900 °C for 3 min. The acetylene gas is decomposed into carbon clusters and hydrogen, and adsorbed on the surface of the nickel nanoparticles in the Si@agarose composites. The decomposed carbon dissolves in the Ni particles and reaches a supersaturated state. Consequently, the dissolved carbon precipitates out by crystallizing in the form of seamless cylinders of CNTs.[37]

Fig. 2a and 2b present the scanning electron microscopy (SEM) images of as-synthesized Si@HC@CNT. The CNTs with tens-of-micrometre length are uniformly covered on the surface of Si@HC (see Fig. S1†). High resolution transmission electron microscopy (HR-TEM) images (shown in Fig. 2c, 2d and 2e) display the morphology and microstructure of CNTs directly grown on HC and Si nanoparticles entirely confined in the HC matrix. The CNTs terminated with Ni particles at their tips (seen with the dark contrast), which indicates that the nanowire growth mechanism follows the tip-growth model. XRD patterns of the Si@HC@CNT also support the presence of CNTs directly grown on Si@HC, as confirmed by HR-TEM (Fig. 2f).[45] Moreover, CNTs are strongly anchored to the surface of Si@HC after the synthesis of Si@HC@CNT (ESI, Fig. S2†). Raman spectroscopy was further used to evaluate the graphitic quality of the Si@HC@CNT (ESI, Fig. S3†). The HC exhibits two obvious peaks at around 1350 and 1585 cm^{-1}, which are attributed to the D and G bands of carbon, respectively.[33] The peak integrated intensity ratio of the D band to the G band (D/G) for Si@HC@CNT was estimated to be 1.74, indicating that most of the carbon species in the Si@HC@CNT were amorphous even though surface of Si@HC was covered CNTs. The elemental analysis showed that the Si@HC@CNT consists of 23 wt% Si, 74 wt% carbon, and 3 wt% Ni.

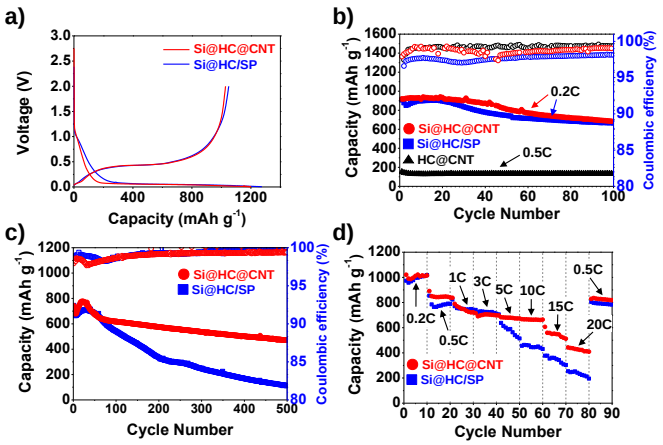

Fig. 3 Electrochemical performances. a) Galvanostatic first cycle discharge/charge curves at a rate of 0.05 C between 0.005 V and 2.0 V; b) Cycle performances of Si@HC@CNT and Si@HC/SP at a rate of 0.2/0.2 C, and HC@CNT at a rate of 0.5 /0.5 C; c) Long cycling retention of of Si@HC@CNT and Si@HC/SP at a rate of 0.5/0.5 C discharge/charge; d) The rate capabilities of each sample (lithiation was fixed at 0.5 C after 11th cycles).

The electrochemical performance of the Si@HC@CNT anodes was investigated by a series of galvanostatic measurements in a coin-type half-cell (2016 R-type). The first discharge (lithiation) and charge (delithiation) capacities are 1148 and 984 mAh g^{-1}, respectively, at a rate of 0.05 C (corresponding to 50 mA g^{-1}) at a voltage range of 0.005 - 2.0 V, corresponding to a high initial coulombic efficiency of 85.7% (Fig 3a). The Si@HC/SP anodes shows the first discharge charge capacity of 1275 mAh g^{-1} with relatively lower initial coulombic efficiency of 82.6% than the Si@HC@CNT. Fig. S4 shows the cyclic voltammograms (CVs) of Si@HC@CNT and Si@HC/SP electrodes obtained at different scan rates (10, 30, and 50 mv s^{-1}) in the potential window of 0 – 3 V after 50 cycles at discharge/charge rate of 0.5 C (ESI, Fig. S4†). The polarization in the Si@HC@CNT electrode was smaller than that of Si@HC/SP, indicating better capacity retention of the Si@HC@CNT.[46]

Both electrodes show stable cycle retention at a low current density at 0.2 C (corresponding to 200 mA g^{-1}) at a voltage range of 0.01 - 2.0 V. This result indicates that HC matrix may effectively accommodate the relatively slow volume change of Si and alleviate the strain/stress of Si nanoparticles during the lithium insertion/deinsertion reaction under the low current density of 200 mA g^{-1}. However, the severe capacity degradation is observed in the Si@HC/SP anodes after only dozens of cycles at a current density at 0.5 C (corresponding to 500 mA g^{-1}). Notably, electrochemical performances of Si-based anodes depend strongly on mass loading.[47] We fabricated anodes with a high-mass-loading of 3.5 mg cm^{-2}. High-mass-loading of battery electrode materials is preferred because it can simplify the number of manufacturing steps.[48] However, the traditional architecture of anode materials on current collectors does not allow for high-mass-loading due to the increase in the cell impedance.[49] As a result, the Si@HC shows the poor cycle performance at a current density at 0.5 C (corresponding to 500 mA g^{-1}), even with addition of 10 wt% conductive agents. On the contrary, the capacity retention of the Si@HC@CNT anodes is significantly enhanced compared to the Si@HC/SP anodes. The good cycle performance of the Si@HC@CNT anodes can be explained as follows: (i) The CNTs directly attached to the Si@HC are effectively connected to each active particle. Consequently, the CNT networks serve as highly conductive 3D networks for the active materials. (ii) One-dimensional (1D) structure of the CNTs provides additional void space for volume expansion of the Si nanoparticles. Thus, the Si@HC@CNT anodes have structural integrity during the rapid volume change under the high current density. And (iii) the CNTs also provide the additional void space for electrolyte penetration, which can enhance the accessibility of lithium ions and electrolytes. For these reasons, the Si@HC@CNT anodes show much improved capacity retention compared to Si@HC/SP anodes during fast discharge/charge process. These positive effects of the CNTs on the electrochemical property are more emphasized at high current density. Fig. 3d shows that the Si@HC@CNT anodes maintain superior capacity retention even at very high rates without notable capacity fading at each rate and especially retain much more enhanced capacity than that of the Si@HC/SP at very high rate (5 - 20 C).

To investigate electrochemical properties of Si@HC@CNT with different CVD times and Si contents, we synthesized Si@HC containing 5 wt% Si and Si@HC@CNT containing 35 wt% Si without CVD process. Si was not observed in Si@HC@CNT (containing 5 wt% of Si) because the Si nanoparticles were fully incorporated in HC matrix (ESI, Fig. S5a†). On the contrary, Si nanoparticles were not fully covered with hard carbon in Si@HC@CNT (containing 35% of Si) (ESI, Fig. S5b†). Due to the presence of Ni catalyst in the samples and high annealing temperature, CNTs were observed in both samples without CVD process. Samples containing 23wt% Si were synthesized at different CVD times. In contrast to Si@HC@CNT obtained without CVD process, most of the particles show largely grown CNTs in the Si/HC composites (ESI, Fig. S6†). Fig. S7 shows the cycle performances of samples with different CVD condition and different Si content (ESI, Fig. S7†). All anodes were prepared with the same loading level (3.5 mg cm^{-2}) of as-synthesized samples. The longer CVD process of the Si@HC shows the higher capacity during the cycles at a current density at 0.5 C (corresponding to 500 mA g^{-1}). However, the coulombic efficiency and specific capacity of the sample with 5 min CVD process was gradually decayed during cycling. Similarly, the higher Si contents in the samples show the higher capacity during the cycling at a current density at 0.5 C (corresponding to 500 mA g^{-1}). However, specific capacity of the sample containing 35 wt% Si was rapidly degraded during cycling. Therefore, appropriate CVD process time (3 min) and Si contents (23 wt%) in the Si@HC@CNT composite were determined to satisfy cycling stability and a high reversible capacity.

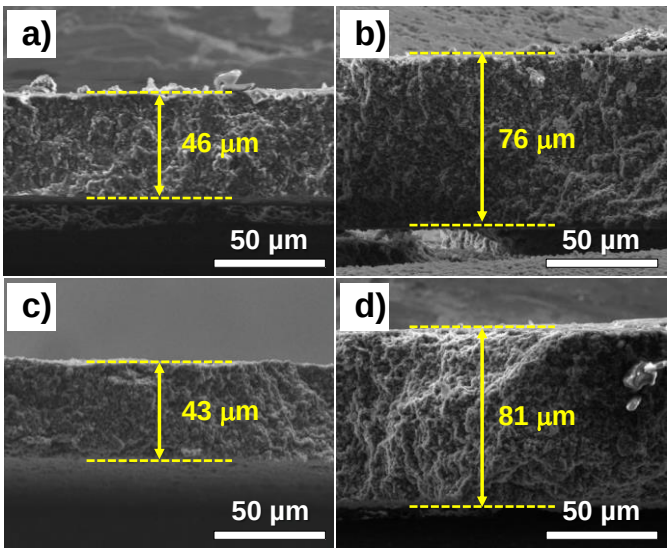

Fig 4. Cross-sectional SEM images of pristine electrodes of a) the Si@HC@CNT and c) the Si@HC/SP, and 100-cycled electrodes of b) the Si@HC@CNT and d) the Si@HC/SP.

As aforementioned, CNTs of the Si@HC@CNT anodes provide additional buffer matrix for volume expansion of the Si nanoparticles, which is clearly seen in the cross-sectional SEM images of the electrodes after 100 cycles at a rate of 0.5 C discharge/charge (Fig. 4). Prior to carrying out electrochemical test, we fabricated all electrodes with the same mass loading (3.5 mg cm^{-2}). Therefore, the pristine Si@HC@CNT anodes exhibit slightly higher thickness than that of the pristine Si@HC/SP anodes. As-expected, the Si@HC@CNT anodes show a significantly reduced volume expansion (65%), compared to that of the Si@HC/SP anodes (88%). These results are attributed to the structure of the interconnected CNTs, in which 1D CNTs and void spaces between them could act as the buffer layer for the large volume expansion during cycling. As

a result, the volume expansion of the Si@HC@CNT anodes is remarkably reduced, compared to that of the Si@HC/SP anodes.

To elucidate the effect of CNTs directly grown on Si@HC further, electrochemical impedance spectroscopy (EIS) was measured. The Nyquist impedance plots are obtained after the 1st and after the 500th cycle for each sample (ESI, Fig. S8†). The semicircle from the high to the medium frequency region is attributed to the contact resistance by the formation of the SEI layer.[50] The medium-frequency semicircle is assigned to the charge transfer resistance, and the straight line in the low-frequency region corresponds to the mass transfer of lithium ions.[11] It is clearly shown that the charge-transfer resistance (R_{ct}) of the Si@HC@CNT anodes is much lower than that of Si@HC/SP anodes after 500 cycles. This finding indicates that the CNT networks maintain improved electronic conductivity after cycling. Moreover, the void space derived from the CNTs facilitates the penetration of lithium ions and electrolytes, which is favourable for lithium ion diffusion.

In summary, we successfully synthesized conductive incorporating Si anodes consisting of directly grown CNTs on HC encapsulating Si nanoparticles via one-pot CVD process. The HC matrix derived from natural polysaccharide offers both conductive and buffer matrix for Si nanoparticles. The CNTs directly attached to Si@HC provide highly conductive 3D networks for the active materials and void space which can not only generate additional buffer space for volume expansion of active materials, but also facilitate the penetration of electrolytes and lithium ions even in the high-mass-loading (3.5 mg cm^{-2}) electrodes. Owing to this novel structure, the Si@HC@CNT anodes showed remarkable improvement in long-term cycle performance in comparison to Si@HC/SP anodes. Furthermore, the Si@HC@CNT anodes exhibit excellent capacity retention even at very high rate (5 - 20 C). We believe that this conductive agent incorporating anode strategy can become a milestone for the fabrication of practical Si-based anodes and also can be extended to other high capacity anode materials such as Ge, GeO_2, SnO_2 and NiO.

Acknowledgements

This work was supported by the BK21 Plus funded by the Ministry of Education, Korea (10Z20130011057).

Notes and references

[a] Department of Energy Engineering, School of Energy and Chemical Engineering, Ulsan National Institute of Science and Technology (UNIST), 50 UNIST-gil, Ulju-gun, Ulsan 689-798, Republic of Korea.
E-mail: spark@unist.ac.kr
[b] Department of Materials Science and Engineering, Korea Advanced Institute of Science and Technology, 291 Daehak-ro, Yuseong-gu, Daejeon 305-701, Republic of Korea.

† Electronic Supplementary Information (ESI) available: SEM images of Si@HC@CNT and Si@HC/SP anodes, Nyquist plots of the electrochemical impedance spectra of both anodes. See DOI:10.1039/xxxx

1 X. Zhou, Z. Dai, S. Liu, J. Bao and Y. G. Guo, *Adv. Mater.*, 2014, **26**, 3943-3949.
2 Z. Zhang, Y. Wang, W. Ren, Q. Tan, Y. Chen, H. Li, Z. Zhong and F. Su, *Angew. Chem. Int. Ed. Engl.*, 2014, **53**, 5165-5169.
3 S. Yuan, X.-L. Huang, D.-L. Ma, H.-G. Wang, F.-Z. Meng and X.-B. Zhang, *Adv. Mater.*, 2014, **26**, 2273-2279.
4 W. Xu, J. Wang, F. Ding, X. Chen, E. Nasybutin, Y. Zhang and J.-G. Zhang, *Energy Environ. Sci.*, 2014, **7**, 513-537.
5 K. Wang, K. Jiang, B. Chung, T. Ouchi, P. J. Burke, D. A. Boysen, D. J. Bradwell, H. Kim, U. Muecke and D. R. Sadoway, *Nature*, 2014, **514**, 348.
6 F.-W. Yuan and H.-Y. Tuan, *Chem. Mater.*, 2014, **26**, 2172-2179.
7 P. Saha, M. K. Datta, O. I. Velikokhatnyi, A. Manivannan, D. Alman and P. N. Kumta, *Prog. Mater Sci.*, 2014, **66**, 1-86.
8 J. H. Cho and S. T. Picraux, *Nano Lett.*, 2014, **14**, 3088-3095.
9 L. Ji, Z. Lin, M. Alcoutlabi and X. Zhang, *Energy Environ. Sci.*, 2011, **4**, 2682.
10 Q. Z. Xiao, Q. Zhang, Y. Fan, X. H. Wang and R. A. Susantyoko, *Energy Environ. Sci.*, 2014, **7**, 2261-2268.
11 S. Xu, C. M. Hessel, H. Ren, R. Yu, Q. Jin, M. Yang, H. Zhao and D. Wang, *Energy Environ. Sci.*, 2014, **7**, 632.
12 D. Wei, M. R. Astley, N. Harris, R. White, T. Ryhanen and J. Kivioja, *Nanoscale*, 2014, **6**, 9536-9540.
13 Y. Wang, G. Xing, Z. J. Han, Y. Shi, J. I. Wong, Z. X. Huang, K. K. Ostrikov and H. Y. Yang, *Nanoscale*, 2014, **6**, 8884-8890.
14 L. L. Tian, X. Y. Wei, Q. C. Zhuang, C. H. Jiang, C. Wu, G. Y. Ma, X. Zhao, Z. M. Zong and S. G. Sun, *Nanoscale*, 2014, **6**, 6075-6083.
15 H. D. Yoo, E. Markevich, G. Salitra, D. Sharon and D. Aurbach, *Mater. Today*, 2014, **17**, 110-121.
16 Q. Z. Xiao, Y. Fan, X. H. Wang, R. A. Susantyoko and Q. Zhang, *Energy Environ. Sci.*, 2014, **7**, 655-661.
17 X. Su, Q. L. Wu, J. C. Li, X. C. Xiao, A. Lott, W. Q. Lu, B. W. Sheldon and J. Wu, *Adv. Energy Mater.*, 2014, **4**, 23.
18 D. M. Piper, J. H. Woo, S.-B. Son, S. C. Kim, K. H. Oh and S.-H. Lee, *Adv. Mater.*, 2014, **26**, 3520-3525.
19 W. Weng, H. J. Lin, X. L. Chen, J. Ren, Z. T. Zhang, L. B. Qiu, G. Z. Guan and H. S. Peng, *J. Mater. Chem. A*, 2014, **2**, 9306-9312.
20 W.-S. Kim, Y. Hwa, J.-H. Shin, M. Yang, H.-J. Sohn and S.-H. Hong, *Nanoscale*, 2014, **6**, 4297-4302.
21 S. Choi, J. C. Lee, O. Park, M. J. Chun, N. S. Choi and S. Park, *J. Mater. Chem. A*, 2013, **1**, 10617-10621.
22 I. Kovalenko, B. Zdyrko, A. Magasinski, B. Hertzberg, Z. Milicev, R. Burtovyy, I. Luzinov and G. Yushin, *Science*, 2011, **334**, 75-79.
23 J. M. Kim, H. S. Park, J. H. Park, T. H. Kim, H. K. Song and S. Y. Lee, *ACS Appl. Mater. Interfaces*, 2014, **6**, 12789-12797.
24 M. S. Wang, W. L. Song, J. Wang and L. Z. Fan, *Carbon*, 2015, **82**, 337-345.
25 D. Mazouzi, D. Reyter, M. Gauthier, P. Moreau, D. Guyomard, L. Roue and B. Lestriez, *Adv. Energy Mater.*, 2014, **4**.
26 K. Fu, Y. Lu, M. Dirican, C. Chen, M. Yanilmaz, Q. Shi, P. D. Bradford and X. Zhang, *Nanoscale*, 2014, **6**, 7489-7495.
27 S. Choi, D. S. Jung and J. W. Choi, *Nano Lett.*, 2014, **14**, 7120-7125.
28 Z. Zhang, M. Zhang, Y. Wang, Q. Tan, X. Lv, Z. Zhong, H. Li and F. Su, *Nanoscale*, 2013, **5**, 5384-5389.
29 M. T. McDowell, S. W. Lee, W. D. Nix and Y. Cui, *Adv. Mater.*, 2013, **25**, 4966-4985.
30 J. I. Lee and S. Park, *Nano Energy*, 2013, **2**, 146-152.
31 S. Jeong, J. P. Lee, G. Kim, M. Ko, S. Park and J. Cho, *Nano Lett.*, 2013, 13, 3403–3407.
32 V. Etacheri, R. Marom, R. Elazari, G. Salitra and D. Aurbach, *Energy Environ. Sci.*, 2011, **4**, 3243-3262.
33 L. M. Sun, X. H. Wang, R. A. Susantyoko and Q. Zhang, *J. Mater. Chem. A*, 2014, **2**, 15294-15297.
34 X. H. Wang, L. N. Sun, R. A. Susantyoko, Y. Fan and Q. Zhang, *Nano Energy*, 2014, **8**, 71-77.
35 X. H. Wang, L. M. Sun, X. N. Hu, R. A. Susantyoko and Q. Zhang, *J. Power Sources*, 2015, **280**, 393-396.
36 C. Kim, M. Ko, S. Yoo, S. Chae, S. Choi, E. H. Lee, S. Ko, S. Y. Lee, J. Cho and S. Park, *Nanoscale*, 2014, **6**, 10604-10610.
37 D. Shao, D. Tang, Y. Mai and L. Zhang, *J. Mater. Chem. A*, 2013, **1**, 15068.
38 L.-G. Cui, L. Hu, J. W. Choi and Y. Cui, *ACS Nano*, 2010, **4**, 3671-3678.
39 X. Li, J.-H. Cho, N. Li, Y. Zhang, D. Williams, S. A. Dayeh and S. T. Picraux, *Adv. Energy Mater.*, 2012, **2**, 87-93.
40 Y. Fan, Q. Zhang, C. Lu, Q. Xiao, X. Wang and B. K. Tay, *Nanoscale*, 2013, **5**, 1503-1506.
41 C. Kim, J. Y. Jang, N. S. Choi and S. Park, *RSC Adv.*, 2014, **4**, 3070-3074.

42 J. P. Tessonnier and D. S. Su, *ChemSusChem*, 2011, **4**, 824-847.
43 M. Kumar and Y. Ando, *J Nanosci Nanotechnol*, 2010, **10**, 3739-3758.
44 Q. Zhang, J. Q. Huang, W. Z. Qian, Y. Y. Zhang and F. Wei, *Small*, 2013, **9**, 1237-1265.
45 H. J. Lin, W. Weng, J. Ren, L. B. Qiu, Z. T. Zhang, P. N. Chen, X. L. Chen, J. Deng, Y. G. Wang and H. S. Peng, *Adv. Mater.*, 2014, **26**, 1217-1222.
46 R. Trocoli, J. Morales and J. S. Pena, *Solid State Ionics*, 2014, **255**, 30-38.
47 Y. K. Jeong, T. W. Kwon, I. Lee, T. S. Kim, A. Coskun and J. W. Choi, *Nano Lett.*, 2014, **14**, 864-870.
48 J.-H. Kim, J.-H. Kim, K.-H. Choi, H. K. Yu, J. H. Kim, J. S. Lee and S.-Y. Lee, *Nano Lett.*, 2014, **14**, 4438-4448.
49 L. Li, Z. Wu, S. Yuan and X. B. Zhang, *Energy Environ. Sci.*, 2014, **7**, 2101-2122.
50 J. Song, S. Chen, M. Zhou, T. Xu, D. Lv, M. L. Gordin, T. Long, M. Melnyk and D. Wang, *J. Mater. Chem. A*, 2014, **2**, 1257.